Proceedings of the
44th IEEE Conference on Decision and Control, and
the European Control Conference 2005
Seville, Spain, December 12-15, 2005

Sensorless Indirect Rotor Field Orientation Speed Control Of Permanent Magnet Synchronous Motor Using Adaptive Rotor Flux Estimator

[1]M Rashed, [1]PFA MacConnell, [1]AF Stronach and [2]P Acarnley

[1]School of Engineering and Physical Sciences, University of Aberdeen, Fraser Noble Building, King's College, Aberdeen, AB24 3UE, Scotland, UK. e-mail: m.rashed@eng.abdn.ac.uk.

[2]Research Engineering Education Services, St Ternan's rectory, Muchalls, Stonehaven, AB39 3PP, Scotland, UK.

Abstract— **Efficient and precise sensorless speed control of Permanent Magnet Synchronous Motor (PMSM) requires accurate knowledge of rotor flux position and speed. In the present paper, an indirect rotor flux oriented scheme for sensorless speed control of PMSM is proposed in which the rotor flux position is estimated by direct integration of the estimated rotor speed to reduce the effect of system noise. The rotor flux magnitude and the rotor flux speed are estimated adaptively using stable Model Reference Adaptive System (MRAS) estimators. Simple stability analysis and design of the estimators are performed using linear control theory. The convergence of rotor position and speed estimation errors to zero is guaranteed. Simulation and experimental results obtained show excellent performance.**

I. INTRODUCTION

High performance operation of PMSM drives mainly relies on the accurate knowledge of the rotor magnet flux magnitude, position and speed. Recently, sensorless PMSM drives are receiving increasing interest in many industrial applications where there are limitations on the use of position sensor. The elimination of the position sensor reduces the cost of the drive and increases the overall system ruggedness and reliability. Sensorless rotor position estimation techniques can be classified into two major groups: the motor model based techniques and the rotor saliency based techniques. The latter is suitable only for Interior PMSM. Most of the motor model based techniques detect the back-EMF vector using open loop estimators [1]-[2] or closed loop estimators/observers [3]-[5]. The back-EMF holds the information of the rotor position and speed. However, this method of calculation introduces measurement noise directly to the estimated position and speed signals. In other motor model based techniques the rotor flux vector is directly estimated instead of the back-EMF [6]. Moreover adaptive observers have been used to estimate the stator current, the rotor speed and the rotor position, [7]-[8]. Extended Kalmen Filter (EKF) has also been proposed for rotor speed and position estimation, [9]-[10]. Although, the EKF algorithm is stable and well known, the EKF is computationally intensive and requires proper initialisation.

In the present paper, an Indirect Rotor Field Oriented Control IRFOC of the PMSM drive is proposed. The rotor flux vector is estimated in its polar form, where the rotor flux vector is completely defined by its magnitude and position. Two MRAS estimators are designed to estimate the rotor speed and the rotor flux magnitude utilising the error between the measured and the estimated stator currents. The rotor flux position is estimated by direct integration of the estimated speed to reduce the effect of measurement noise. In comparison to the conventional approaches, the MRAS estimators developed in this paper are simple to implement and robust to system noise. The two MRAS estimators are designed to provide stable operation on an independent and simultaneous use basis. Stability analysis and design of the MRAS estimators have been performed to a linearised PMSM model in a synchronous rotating reference frame fixed to the estimated rotor flux vector. The convergence of the estimated rotor position and speed to their true values is guaranteed.

The model of the PMSM in stationary and synchronous rotating reference frames is discussed in section 2. In section 3, the sensorless adaptive rotor flux vector estimation scheme is designed and discussed. Detailed simulation results are given in section 4. Also, experimental results have been obtained and are given in Section 5. Finally, conclusions are drawn and presented in section 6.

II. PMSM MODEL

The linear state space model of a surface mounted PMSM in a stationary reference frame (sD, sQ) fixed to the stator windings, is given as [6]:

$$\dot{\bar{\psi}}_r = \boldsymbol{J}\omega_r\bar{\psi}_r \tag{1a}$$

$$\dot{\bar{i}}_s = -a_1\boldsymbol{I}\bar{i}_s - \boldsymbol{J}a_2\omega_r\bar{\psi}_r + a_2\bar{u}_s \tag{1b}$$

where: $\bar{u}_s = \begin{bmatrix} u_{sD} & u_{sQ} \end{bmatrix}^T$, $\bar{i}_s = \begin{bmatrix} i_{sD} & i_{sQ} \end{bmatrix}^T$, $\bar{\psi}_r = \begin{bmatrix} \psi_{rD} & \psi_{rQ} \end{bmatrix}^T$,

$\psi_r = \sqrt{\psi_{rD}^2 + \psi_{rQ}^2}$, $\psi_{rD} = \psi_r \cos\rho_r$, $\psi_{rQ} = \psi_r \sin\rho_r$,

$\rho_r = \int \omega_r dt$, $a_1 = \dfrac{R_s}{L_s}$, $a_2 = \dfrac{1}{L_s}$, $\boldsymbol{J} = \begin{bmatrix} 0 & -1 \\ 1 & 0 \end{bmatrix}$, $\boldsymbol{I} = \begin{bmatrix} 1 & 0 \\ 0 & 1 \end{bmatrix}$

$\bar{\psi}_r$ rotor flux space vector, $\bar{i}_s$ stator current space vector, $\bar{u}_s$ stator voltage space vector, ω_r rotor angular speed in electrical rad/s, ρ_r rotor position, ψ_r actual rotor (magnet) flux magnitude, R_s stator winding resistance and L_s stator winding inductance. The motor state variables are two-stator currents i_{sD} and i_{sQ} and two rotor fluxes ψ_{rD} and ψ_{rQ}. The system inputs are the stator voltages u_{sD} and u_{sQ}. The system outputs are i_{sD} and i_{sQ}. (1b) represents the motor stator circuit model. (1a) represents the rotor model, which is completely decoupled from (1b) since the rotor flux is provided by a permanent magnet. It is well known that the design and the analysis of estimators/observers in the synchronous rotating reference frames is much simpler than in the stator windings reference frame since in the synchronous reference frame the

0-7803-9568-9/05/$20.00 ©2005 IEEE

sinusoidal time varying variables of the PMSM will be transformed to DC variables. In the synchronous rotating reference frame (x, y) that rotates at speed ω_e, the motor model in (1) is written as:

$$\dot{\bar{\psi}}_r = -\boldsymbol{J}(\omega_{sl})\bar{\psi}_r \tag{2a}$$

$$\dot{\bar{i}}_s = -(a_1\boldsymbol{I} + \omega_e\boldsymbol{J})\bar{i}_s - \boldsymbol{J}a_2\omega_r\bar{\psi}_r + a_2\bar{u}_s \tag{2b}$$

where: $\bar{u}_s = \begin{bmatrix} u_{sx} & u_{sy} \end{bmatrix}^T$, $\bar{i}_s = \begin{bmatrix} i_{sx} & i_{sy} \end{bmatrix}^T$, $\bar{\psi}_r = \begin{bmatrix} \psi_{sx} & \psi_{sy} \end{bmatrix}^T$, $\psi_r = \sqrt{\psi_{rx}^2 + \psi_{ry}^2}$, $\omega_e = d\rho_e/dt$; $\omega_{sl} = (\omega_e - \omega_r)$, ρ_e position of rotating reference frame in electrical rad. ω_e synchronous rotating reference frame speed in electrical rad/s. In the next section the rotor speed and the rotor flux magnitude estimators will be presented.

III. Adaptive Rotor Flux Vector Estimator

In the synchronous rotating reference frame the estimated version of the PMSM model in (2) may be expressed as follows:

$$\dot{\hat{\bar{\psi}}}_r = -\boldsymbol{J}(\hat{\omega}_{sl})\hat{\bar{\psi}}_r \tag{3a}$$

$$\dot{\hat{\bar{i}}}_s = -(\hat{a}_1\boldsymbol{I} + \omega_e\boldsymbol{J})\hat{\bar{i}}_s - \boldsymbol{J}a_2\hat{\omega}_r\hat{\bar{\psi}}_r + a_2\bar{u}_s \tag{3b}$$

where: $\hat{\omega}_{sl} = (\omega_e - \hat{\omega}_r)$, "$\wedge$" denotes an estimated quantity.

By subtracting (3a) and (3b) from (2a) and (2b) respectively and by applying Laplace transform, an estimation error model of the PMSM in the synchronous rotating reference frame is given as:

$$\begin{bmatrix} \Delta\psi_{rx} \\ \Delta\psi_{ry} \end{bmatrix} = \frac{1}{s^2 + \omega_{sl}^2}\begin{bmatrix} (-\hat{\psi}_{ry}s + \omega_{sl}\hat{\psi}_{rx}) \\ (\hat{\psi}_{rx}s + \omega_{sl}\hat{\psi}_{ry}) \end{bmatrix}\Delta\omega_r \tag{4a}$$

$$\begin{bmatrix} \Delta i_{sx} \\ \Delta i_{sy} \end{bmatrix} = \frac{-1}{D}\left\{\begin{bmatrix} \hat{i}_{sx}F + \hat{i}_{sy}\omega_e \\ \hat{i}_{sy}F - \hat{i}_{sx}\omega_e \end{bmatrix}\Delta a_1 + a_2\begin{bmatrix} \hat{\psi}_{rx}\omega_e - \hat{\psi}_{ry}F \\ \hat{\psi}_{rx}F + \hat{\psi}_{ry}\omega_e \end{bmatrix}\Delta\omega_r + a_2\begin{bmatrix} \omega_r\omega_e & -\omega_r F \\ \omega_r F & \omega_r\omega_e \end{bmatrix}\begin{bmatrix} \Delta\psi_{rx} \\ \Delta\psi_{ry} \end{bmatrix}\right\} \tag{4b}$$

where: $\Delta\bar{\psi}_r = \bar{\psi}_r - \hat{\bar{\psi}}_r = \begin{bmatrix} \Delta\psi_{rx} & \Delta\psi_{ry} \end{bmatrix}^T$, $\Delta\omega_r = (\omega_r - \hat{\omega}_r)$

$\Delta\bar{i}_s = \bar{i}_s - \hat{\bar{i}}_s = \begin{bmatrix} \Delta i_{sx} & \Delta i_{sy} \end{bmatrix}^T$, $\Delta a_1 = (a_1 - \hat{a}_1)$

$\Delta i_{sx} = (i_{sx} - \hat{i}_{sx})$, $\Delta i_{sy} = (i_{sy} - \hat{i}_{sy})$, $\Delta\psi_{rx} = (\psi_{rx} - \hat{\psi}_{rx})$,

$\Delta\psi_{ry} = (\psi_{ry} - \hat{\psi}_{ry})$, $\omega_r\bar{\psi}_r - \hat{\omega}_r\hat{\bar{\psi}}_r = \omega_r\Delta\bar{\psi}_r + \Delta\omega_r\hat{\bar{\psi}}_r$,

$D = F^2 + \omega_r^2$, $F = (s + a_1)$.

The stator current errors Δi_{sx} and Δi_{sy} are utilised to adaptively estimate the rotor speed ω_r and the rotor flux magnitude ψ_r using MRAS estimators where the actual PMSM drive (as a reference model) and its implemented model inside the drive controller (as an adjustable model) are operated in parallel as shown in Fig 1. The (adjustable) model of the PMSM implemented inside the control algorithm should strictly include the effects of harmonics in the spatial distribution of the magnet flux and of the air-gap reluctance variations due to the stator slots. These effects are sources of current harmonics and torque pulsations. However, the PMSM used for the experimental investigation had a sinusoidally distributed magnet flux and skewed stator slots, so the flux harmonics and air-gap reluctance variations are negligible and thus the ideal machine model can be used. Inside the controller of the IRFOC PMSM drive, the synchronous rotating reference frame is assumed fixed to the estimated rotor flux vector and thus the estimated rotor flux vector components are: $\hat{\psi}_{rx} = \hat{\psi}_r$ and $\hat{\psi}_{ry} = 0$. Therefore, from (3b), the estimate of the stator currents and the rotor position are implemented inside the controller of the sensorless IRFOC PMSM drive as follows:

$$\dot{\hat{i}}_{sx} = -\hat{a}_1\hat{i}_{sx} + \omega_e\hat{i}_{sy} + a_2u_{sx} \tag{5a}$$

$$\dot{\hat{i}}_{sy} = -\hat{a}_1\hat{i}_{sy} - \omega_e\hat{i}_{sx} - a_2\hat{\omega}_r\hat{\psi}_r + a_2u_{sy} \tag{5b}$$

$$\hat{\omega}_{sl} = 0;\ \omega_e = \hat{\omega}_r;\ \hat{\rho}_r = \int\hat{\omega}_r dt \tag{5c}$$

Fig 2 shows the block diagram of the proposed sensorless IRFOC PMSM drive. For small perturbations around the equilibrium point, it is assumed that $\omega_{sl} \rightarrow \hat{\omega}_{sl} = 0$. Thus by substituting $\omega_{sl} = 0$ and $\hat{\psi}_{ry} = 0$ into (4) and eliminating $\Delta\psi_{ry}$ from (4b), yields:

$$\begin{bmatrix} \Delta i_{sx} \\ \Delta i_{sy} \end{bmatrix} = \frac{1}{D}\left\{\begin{bmatrix} -\hat{i}_{sx}F - \hat{i}_{sy}\omega_r \\ -\hat{i}_{sy}F + \hat{i}_{sx}\omega_r \end{bmatrix}\Delta a_1 - a_2\begin{bmatrix} \omega_r^2 \\ \omega_r F \end{bmatrix}\Delta\psi_{rx} + \frac{a_2}{s}\begin{bmatrix} a_1\omega_r\hat{\psi}_r \\ -\hat{\psi}_r(s^2 + a_1 s + \omega_r^2) \end{bmatrix}\Delta\omega_r\right\} \tag{6}$$

The stator current error vector components Δi_{sx} and Δi_{sy} from (6) are then utilised to derive the adaptive error signals ε_ω and ε_ψ that are fed to PI type controllers to estimate adaptively ω_r and ψ_r respectively. The selection of these adaptive error signals will be discussed in the next section.

A. Rotor Speed and Rotor Flux Magnitude Estimators

From (6), the adaptive error signals ε_ω and ε_ψ are chosen as follows:

$$\varepsilon_\omega = -\Delta i_{sy}/(a_2\hat{\psi}_r) \tag{7a}$$

$$\varepsilon_\psi = -\Delta i_{sx}/(a_2\omega_r^2) \tag{7b}$$

The adaptive error signal equations in (7) are chosen according to the following rules:

- It should be a set of linearly independent equations of Δi_{sx} and Δi_{sy}.
- The poles and the zeros of the transfer functions $(\varepsilon_\omega/\Delta\omega_r)$ and $(\varepsilon_\psi/\Delta\psi_r)$ should be located in the left hand side of the s-plane at any operating point.
- The gains of these transfer functions are unity.

The adaptive error signals are fed to PI type controllers. Thus:

$$\hat{\omega}_r = G_{c\omega}\varepsilon_\omega \tag{8a}$$

$$\hat{\psi}_r = G_{c\psi}\varepsilon_\psi \tag{8b}$$

where: $G_{c\omega} = k_{p\omega} + k_{i\omega}/s$, $G_{c\psi} = k_{p\psi} + k_{i\psi}/s$. $k_{p\omega}$, $k_{i\omega}$, $k_{p\psi}$ and $k_{i\psi}$ are the MRAS estimators PI controllers gains.

B. Stability Analysis and Design of the Estimators

By substituting from (6) about Δi_{sx} and Δi_{sy} into (7), ε_ω and ε_ψ may be expressed as function of $\Delta\omega_r$, $\Delta\psi_{rx}$ and Δa_1 as follows:

$$\begin{bmatrix}\varepsilon_\omega\\ \varepsilon_\psi\end{bmatrix}=\begin{bmatrix}G_{\omega\omega} & G_{\omega\psi}\\ G_{\psi\omega} & G_{\psi\psi}\end{bmatrix}\begin{bmatrix}\Delta\omega_r\\ \Delta\psi_{rx}\end{bmatrix}+\begin{bmatrix}G_{\omega a1}\\ G_{\psi a1}\end{bmatrix}\Delta a_1 \quad (9)$$

where: $G_{\omega\omega}=\dfrac{\left(s^2+a_1 s+\omega_r^2\right)}{sD}$; $G_{\omega\psi}=\dfrac{\omega_r F}{\hat{\psi}_r D}$; $G_{\psi\omega}=-\dfrac{a_1\hat{\psi}_r}{\omega_r sD}$

$$G_{\omega a1}=\frac{\hat{i}_{sy}F-\hat{i}_{sx}\omega_r}{a_2\hat{\psi}_r D};\ G_{\psi\psi}=\frac{1}{D}\ G_{\psi a1}=\frac{\hat{i}_{sx}F+\hat{i}_{sy}\omega_r}{a_2\omega_r^2 D}$$

The rotor speed and the rotor flux magnitude estimators given by (7-9) are represented by the 2×2 MIMO closed loop control system shown in Fig 3. The design of the PI controller of each estimator is performed on an independent use basis where each estimator is treated as a Single Input Single Output (SISO) closed loop control system. As an example, the rotor speed estimator is designed by assuming the effect of $\Delta\psi_{rx}$ and Δa_1 a bounded external disturbance. However, stability will not be guaranteed for simultaneous use of the estimators. Therefore, stability of the designed estimators should be also investigated for the simultaneous use case. The block diagram in Fig 3a shows the closed loop control system of the rotor speed estimator. Before proceeding to determine the speed PI controller gains, it should be noted that the existence of a $G_{\omega\omega}$ pole at the origin of the s-plane ensures the convergence of the $\Delta\omega_r$ to zero despite the value of the disturbance signal, see Fig 3a. This agrees with the physical interpretation that at steady state the rotor speed will be exactly equal to the estimated value since ω_e is set equal to the estimated speed in the proposed IRFOC PMSM drive, (5c). The feed-forward transfer function of the speed estimator, Fig 3a is:

$$\hat{\omega}_r/\Delta\omega_r=G_{c\omega}G_{\omega\omega} \quad (10)$$

It has 4 poles FFP1-4 and 3 zeros FFZ1-3. These are: FFP1,2 = 0; FFP3,4 = $-a_1 \pm j\omega_e$; FFZ1 = $-k_{i\omega}/k_{p\omega}$ and FFZ2, 3 = $-0.5a_1 \pm 0.5sqrt(a_1^2-4\omega_e^2)$ as indicated in Fig 4. The locations of the closed loop transfer function poles CLP characterize the control system dynamics. The location of the PI controller zero FFZ1 is chosen to be on the real axis at $-a_1$ to make sure that the fast dynamics CLP are always located to the left of the conjugate poles FFP3-4. This will provide a quick transient response. The $k_{p\omega}$ can be selected to be as large as possible to give tie tracking to the actual motor speed. The PI controller gains are chosen as: $k_{i\omega}/k_{p\omega}= a_1$ and $k_{p\omega}$ = 300. The root locus of the speed estimator for the motor parameters given in Appendix A is plotted in Fig 4 at operating point of i_{sx} = 0 A, i_{sy} = 2 A, $k_{i\omega}/k_{p\omega}= a_1$ and ω_e = 150 elect. rad/s. The closed loop poles when $k_{p\omega}$ = 300 are indicated by CLP1-4. The block diagram in Fig 3b shows the closed loop control system of the rotor flux magnitude estimator. Similar to the speed estimator, the feed-forward transfer function of the rotor flux magnitude estimator is:

$$\hat{\psi}_r/\Delta\psi_{rx}=G_{c\psi}G_{\psi\psi} \quad (11)$$

It has 3 poles FFP1-3 and 1 zero FFZ1 as shown in Fig 5. The first pole FFP1 is at the origin. The other two poles are: FFP2, 3 = $-a_1 \pm j\omega_e$. The zero FFZ1 is the PI controller zero and is: FFZ1 = $-k_{i\psi}/k_{p\psi}$. The FFZ1 is selected close to the origin in order to reduce the dominance of the first closed loop pole CLP1. $k_{i\psi}/k_{p\psi}$ is selected equal to 20 and $k_{p\psi}$ = 5000. Root locus is plotted for the rotor flux magnitude estimator when i_{sx} = 0, i_{sy} = 2 A and $k_{i\psi}/k_{p\psi}$ = 20 for speed of 150 elect. rad/s. The root locus is shown in Fig 5. The closed loop poles when $k_{p\psi}$ = 5000 are indicated by CLP1-3. In the next section, the stability of the estimators as a 2×2 MIMO will be investigated.

C. MIMO Stability Investigation

In this section the stability of the two estimators on simultaneous use basis as a 2×2 MIMO system is investigated using the selected PI controller gains obtained in the previous section. This is performed by investigating the locations of the closed loop poles of the 2×2 MIMO system in Fig 3. From Fig 3, the relationship between the system outputs $\hat{\omega}_r$ and $\hat{\psi}_r$ and the errors $\Delta\omega_r$ and $\Delta\psi_{rx}$, which represents the feed-forward transfer function of the 2×2 MIMO system, is given as follows:

$$\begin{bmatrix}\hat{\omega}_r\\ \hat{\psi}_r\end{bmatrix}=\begin{bmatrix}G_{c\omega} & 0\\ 0 & G_{c\psi}\end{bmatrix}\left\{\begin{bmatrix}G_{\omega\omega} & G_{\omega\psi}\\ G_{\psi\omega} & G_{\psi\psi}\end{bmatrix}\begin{bmatrix}\Delta\omega_r\\ \Delta\psi_r\end{bmatrix}+\begin{bmatrix}G_{\omega a1}\\ G_{\psi a1}\end{bmatrix}\Delta a_1\right\} \quad (12)$$

The effect of the error Δa_1 in (12) is assumed to be a bounded external disturbance, and so is ignored for stability study. The locations of the closed loop poles of the 2×2 MIMO system are obtained by solving the following characteristic equation:

$$\left|\boldsymbol{I}+\begin{bmatrix}G_{c\omega} & 0\\ 0 & G_{c\psi}\end{bmatrix}\begin{bmatrix}G_{\omega\omega} & G_{\omega\psi}\\ G_{\psi\omega} & G_{\psi\psi}\end{bmatrix}\right|=0 \quad (13)$$

The poles of (13) are numerically calculated for a range of speeds from ±0.1 up to ±314 elect. rad/s. The locus of these poles is plotted in Fig 6. The points indicated by crosses in Fig 6 are the locations of the seven poles of the characteristic equation at ω_r = ± 0.1 elect. rad/s. As the speed increases, the poles' locations move in the directions indicated by the arrows. The locus obtained is located in left hand side of the s-plane for the whole speed range of operation and for any value of i_{sx} and i_{sy}. Therefore, the designed estimators will also provide stable operation for simultaneous use.

D. Proof of Convergence

Stable operation of the two estimators on both independent and simultaneous use basis is guaranteed as demonstrated in the previous section. However, it is crucial for high-performance/efficient operation of sensorless PMSM drive that the steady state errors of the estimated quantities converge to zero. At steady state, the adaptive error signals ε_ω, and ε_ψ are equal to zero since they are fed to PI controllers. In addition the speed error $\Delta\omega_r$ is equal to zero as has been explained in section III.A. Thus, by substituting (4b) into (7) and substituting the operator s = 0, yields:

$$\varepsilon_\omega=\left(a_1 i_{sy}-\omega_r i_{sx}\right)\Delta a_1+a_1 a_2\omega_r\Delta\psi_{rx}+a_2\omega_r^2\Delta\psi_{ry}=0 \quad (14a)$$

$$\varepsilon_\psi=\left(-a_1 i_{sx}-\omega_r i_{sy}\right)\Delta a_1-a_2\omega_r^2\Delta\psi_{rx}+a_1 a_2\omega_r\Delta\psi_{ry}=0 \quad (14b)$$

By solving (14), the rotor flux vector error components as functions of Δa_1 are:

$$\Delta\psi_{ry}=\left(i_{sx}/a_2\omega_r\right)\Delta a_1 \quad (15a)$$

$$\Delta\psi_{rx}=-\left(i_{sy}/a_2\omega_r\right)\Delta a_1 \quad (15b)$$

It should be noted from (15) that if i_{sx} is zero, $\Delta\psi_{ry} \rightarrow 0$ and thus, the rotor position error is zero (since $\psi_{ry} = 0$) despite the value of the stator resistance mismatch. Therefore, i_{sx} reference value is set to zero in order to cancel the influence of the stator resistance mismatch on the steady state error of the estimated rotor position. It should be also noted that the error $\Delta\psi_{rx}$ is equal to the difference between the actual and the estimated value of the rotor flux magnitude and is sensitive to Δa_1. The error $\Delta\psi_{rx}$ increases to a large extent as the speed decreases down to zero. However, the influence of Δa_1 is small at high speeds. In order to obtain stable and accurate flux estimation, the stator resistance should also be estimated. This will be considered in future publication.

IV. Simulation Results

The proposed sensorless IRFOC PMSM drive incorporating the designed rotor speed and rotor flux magnitude MRAS estimators has been simulated using Matlab/Simulink. The block diagram in Fig 2 illustrates the simulated drive. In this drive the stator current is estimated using (5). The rotor speed is estimated using (8a) and the rotor flux magnitude is estimated using (8b). Extensive simulation work has been carried out to investigate the performance and the stability of the proposed PMSM drive. The parameters of the PMSM used are given in Appendix A.

Fig 7 shows simulation results for starting and reversal of the drive in sensorless speed control mode. The reference speed is set to 2 rad/s at t = 0.5 s and reversed to –2 rad/s at t = 5 s. A constant load torque of 2 Nm is applied to the drive. The results obtained show stable operation and accurate estimate of the rotor speed, the rotor position and the rotor flux magnitude. The estimated rotor flux magnitude is intentionally increased at t = 2 s inside the controller by 10% of its nominal value. The rotor flux magnitude estimator was able to recover the estimated rotor flux magnitude to its true value. Furthermore, in Fig 8, results are shown for operation at higher speed of 20 rad/s where the value of the stator resistance is suddenly reduced by 20% of its nominal value at t = 2 s. It is noted that after the transient period the estimated rotor speed and position are converged to their true value while the estimated rotor flux magnitude has a small steady state error, (15b).

V. Experimental Results

The algorithm of the proposed sensorless IRFOC PMSM drive incorporating the designed rotor speed and rotor flux magnitude MRAS estimators has been implemented on a TMS320C31 DSP platform. The switching and the sampling times are equal to 100 μs. The stator voltage is reconstructed by using the PWM pulses and the measured DC link voltage. In addition, an algorithm is used to compensate the effect of the inverter non-linearities, i.e. the dead time and the transistors' voltage drops, [11]. The discussion of the algorithm is beyond the scope of this paper. The stator current is estimated using (5). The rotor speed and the rotor flux magnitude are estimated using (8a) and (8b) respectively. The parameters of the PMSM used are given in Appendix A.

A crane type load loads the drive. The drive is used to lift up and lower down a constant weight. During lifting up phase the PMSM operates in motoring mode while it operates in generating mode during lowering down phase. The drive is operated to lift up a weight of 15 kg at low speed of 2 rad/s. The estimators are activated while the stator resistance is set to its nominal value. The reference value of i_{sx} is set equal to zero. The results are shown in Fig 9. At t = 0 s, the speed is reversed to –2 rad/s to lower down the load. It is noted that, the average value of the rotor position error is converged to zero as shown in Fig 9c. Despite the high system noise to signal ratio at such low speed operation, the results show stable operation in motoring and generating modes. With an improved inverter non-linearities compensation algorithm, smoother and smaller ripple signals can be obtained at low speeds. The torque current component i_{sy} is shown in Fig 9e. During lifting up period, i_{sy} was higher than 3 A, which corresponds to 90% of the rated torque of the motor. In the lowering down period, i_{sy} is less than 3 A because the crane pulley friction torque component is reversed. The estimated rotor flux magnitude is shown in Fig 9d.

Another type of test is carried out to show the convergence of the estimated rotor position to the true value during start up of the drive. In this test the PMSM motor is coupled to a DC generator, which acts as a load. The DC generator terminals are connected to a resistor. The reference speed is set to 10 rad/s. The initial rotor position error is set to +1.2 rad. The drive and the estimators are started up at t = 0 s. The results are shown in Fig 10. It can be seen from Fig 10c that the rotor position error converges quickly to zero. It can also be seen from the results that at higher speed operation the noise to signal ratio is less.

In addition, the drive is investigated for no-load operation. In this test the shaft of the PMSM is completely decoupled from the shaft of the DC generator and left to run free of load. A speed reversal test from 2 to –2 rad/s is carried out. The results obtained are shown in Fig 11. The results show stable operation. The average value of the rotor position error is converged to zero. Although, i_{sy} is very small (Fig 11e) stable estimation is still possible.

The experimental investigation has shown stable operation of the drive at low speeds for loaded and no-load cases. Also, It has been shown that the rotor position estimation is robust to the initial position error at start up of the drive.

VI. Conclusions

The proposed sensorless IRFOC PMSM drive provides rotor position estimates immune to system noise and accurate speed estimates insensitive to the machine parameters mismatch. The rotor speed and the rotor flux magnitude have been regarded as slowly varying parameters, which have been adaptively estimated using two MRAS estimators. The rotor position is estimated by direct integration of the estimated rotor speed. Stability analysis and design based on linear control theory have been performed for the proposed MRAS estimators on an independent and simultaneous use basis. The convergence of the estimated quantities to their true values is also guaranteed on condition that the other machine parameters are accurately known. The convergence

of the estimated rotor position to its true value always occurs despite the value of the stator resistance mismatch if i_{sx} is equal to zero. Simulation and experimental investigations of the drive demonstrate accurate and stable position/speed estimation in the various operating modes.

APPENDIX A

PMSM Parameters:

Connection Type: Y	Frequency: 50 Hz
Voltage Rating: 380 V	L_s = 0.02 H
Current Rating: 3.5355 A	R_s= 3.58356 Ω
Number of Phases: 3ph	$\psi_{r\text{-}n}$ = 0.2592772 Web
Number of poles: 6	$T_{e\text{-}max}$ = 5 Nm
Rated speed: 3000 rpm	$T_{e\text{-}n}$ = 3.9 Nm

REFERENCES

[1] Kim J and Sul S: New Approach for High Performance PMSM Drives without Rotational Position Sensors, *IEEE Trans. Power Electronics*, Vol. 12, September 1997, pp. 904-911.

[2] Matsui N and Shigyo M: Brushless dc Motor Control without Position and Speed Sensores, *IEEE Trans. Industry Applications*, Vol.28, No. 1, January/February 1992, pp. 120-127.

[3] Solsona J and Valla MI: Disturbance and Nonlinear Luenberger Observers for Estimating Mechanical Variables in Permanent Magnet Synchronous Motors Under Mechanical Parameters Uncertainties, *IEEE Trans. Industrial Electronics*, Vol. 50, No. 4, August 2003, pp. 717-725.

[4] Tomita M, Senjyu T, doki S and Okuma S: New Sensorless Control for Brushless DC Motors Using Disturbance Observers and Adaptive Velocity Estimators, *IEEE Trans. Industrial Electronics*, Vol. 45, No. 2, April 1998, pp. 274-282.

[5] Ichikawa S, Chen Z, Tomita M, Doki S and Okuma S: Sensorless Controls of Salient-Pole permanent Magnet Synchronous Motors Using Extended Electromotive Force Models, *Electrical Engineering in Japan*, Vol. 146, No. 3, 2004, pp. 55-64.

[6] Chen Z, Tomita M, Doki S and Okuma S: New Adaptive Sliding Observers for Position and Velocity-Sensorless Controls of Brushless DC Motors, *IEEE Trans. Industrial Electronics*, Vol. 47, No. 3, June 2000, pp. 582-591.

[7] Jones LA and Lang JH: Astate Observer for the Permanent-Magnet Synchronous Motor, *IEEE Trans. Industrial Electronics*, Vol. 36, No. 3, August 1989, pp. 374-382

[8] Sepe RB and Lang JH: Real-Time Observer-Based (Adaptive) Control of a Permanent-Magnet Synchronous Motor without Mechanical Sensors, *IEEE Trans. Industry Applications*, Vol. 28, No. 6, November 1992, pp. 1345-1352.

[9] Bolognani S, Oboe R and Zigliotto M: Sensorless Full-Digital PMSM Drive With EKF Estimation of Speed and Rotor Position, *IEEE Trans. Industrial Electronics*, Vol. 46, No. 1, February 1999, pp. 184-191.

[10] Dhaouadi R, Mohan N and Norum L: Design and Implementation of an Extended Kalman Filter for the State Estimation of a Permanent Magnet Synchronous Motor, *IEEE Trans. Power Electronics*, Vol. 6, No. 3, July 1991, pp. 491-497.

[11] Choi JW and Sul SK: Inverter Output Voltage Synthesis Using Novel Dead Time Compensation, *IEEE Trans. Power Electronics*, Vol. 11, No. 2, March 1996, pp. 221-227.

LIST OF FIGURES

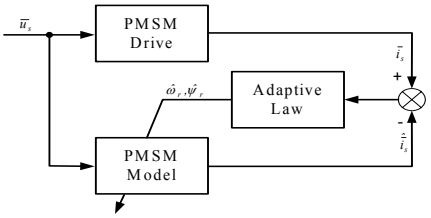

Fig. 1 MRAS block diagram

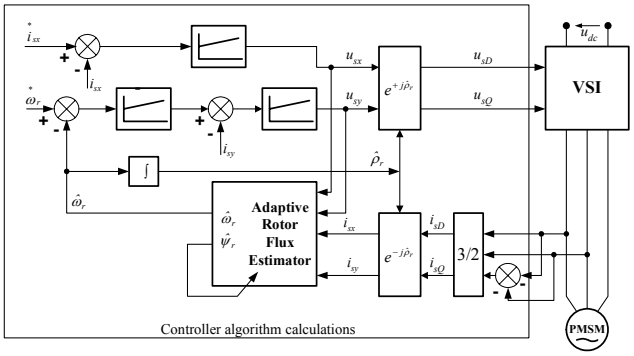

Fig. 2 Sensorless IRFOC PMSM drive.

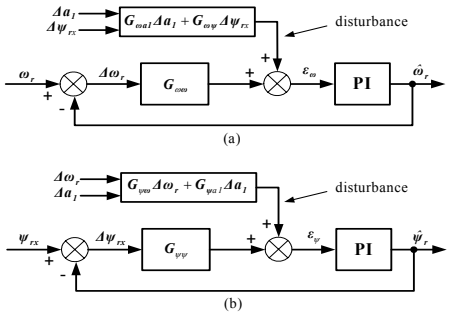

Fig. 3 Motor speed and rotor flux magnitude estimators block diagram.

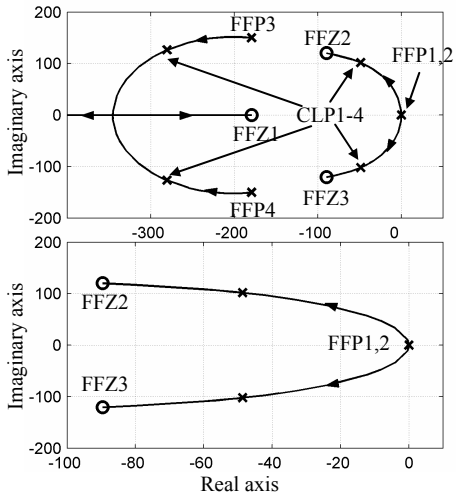

Fig. 4 Root locus of rotor speed estimator, ω_e = 150 elect. rad/s. Top subplot: complete root locus. Bottom subplot: Zoom in at the origin.

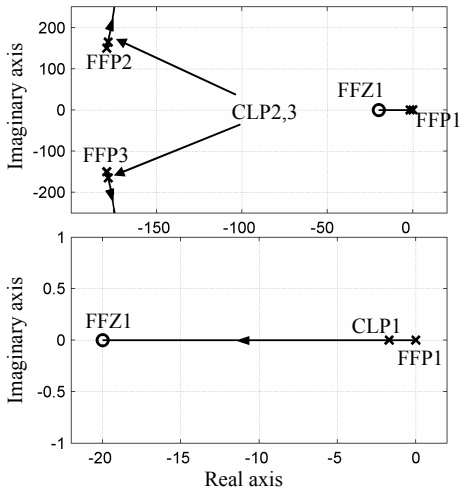

Fig. 5 Root locus of Rotor flux magnitude estimator, ω_e = 150 elect. rad/s. Top subplot: complete root locus. Bottom subplot: Zoom in at the origin.

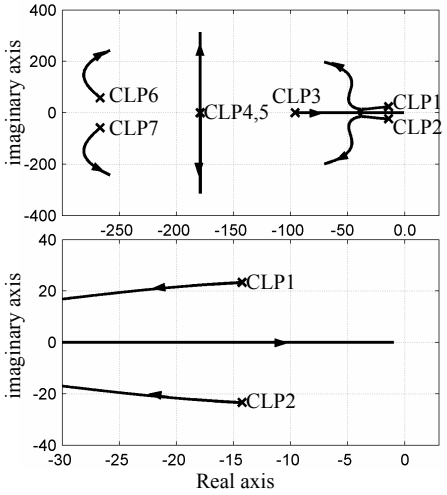

Fig. 6 Locus of closed loop poles of speed and rotor flux magnitude estimators on simultaneous use basis. $\omega_e = \pm 0.1 \rightarrow \pm 314$ elect. rad/s. Top subplot: Complete Locus. Bottom subplot: Zoom in at the origin.

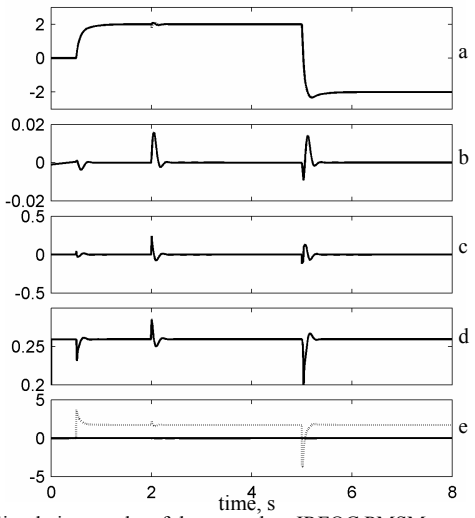

Fig. 7 Simulation results of the sensorless IRFOC PMSM. a: —ω_r and … $\hat{\omega}_r$ rad/s. b: $\Delta\rho_r$ rad. c: $\Delta\omega_r$ rad/s. d: $\hat{\psi}_r$ Web. e: —i_{sx} and …i_{sy} A.

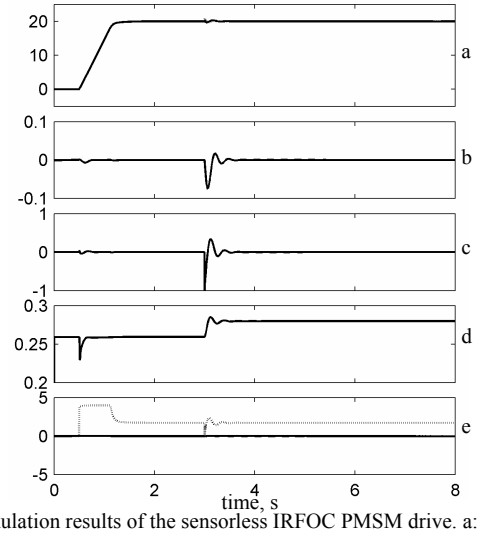

Fig. 8 Simulation results of the sensorless IRFOC PMSM drive. a: —ω_r and … $\hat{\omega}_r$ rad/s. b: $\Delta\rho_r$ rad. c: $\Delta\omega_r$ rad/s. d: $\hat{\psi}_r$ Web. e: —i_{sx} and …i_{sy} A.

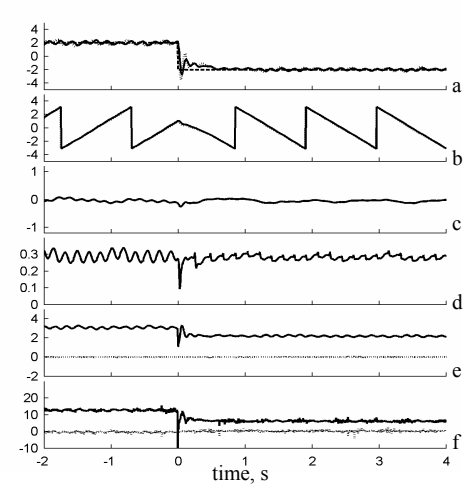

Fig. 9 Experimental Results. a: -- ω_r^* , — $\hat{\omega}_r$ and …ω_r mech. rad/s. b: …ρ_r and — $\hat{\rho}_r$, elect. rad/s. c: $\Delta\rho_r$, elect. rad/s. d: $\hat{\psi}_r$, Web. e: …i_{sx} and — i_{sy}, A. f: …u_{sx} and — u_{sy}, V.

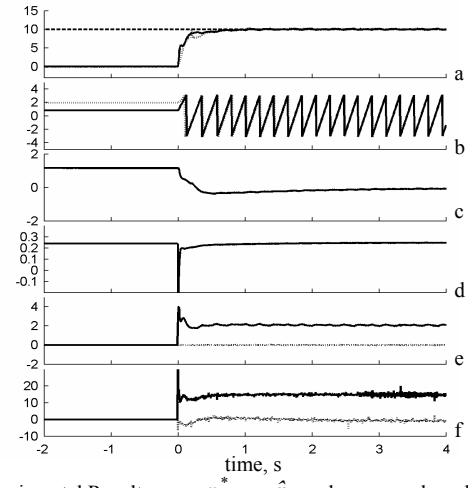

Fig. 10 Experimental Results. a: -- ω_r^* , — $\hat{\omega}_r$ and …ω_r mech. rad/s. b: …ρ_r and — $\hat{\rho}_r$, elect. rad/s. c: $\Delta\rho_r$, elect. rad/s. d: $\hat{\psi}_r$, Web. e: …i_{sx} and — i_{sy}, A. f: …u_{sx} and — u_{sy}, V.

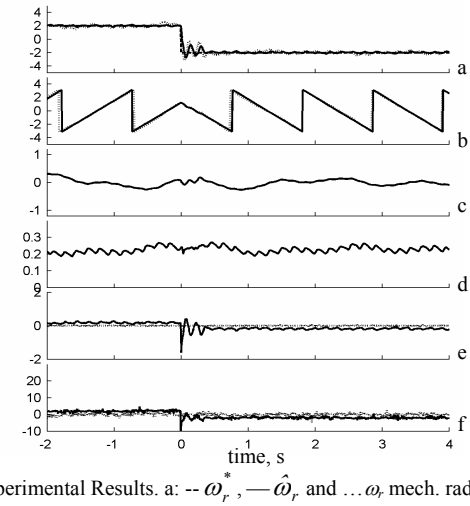

Fig. 11 Experimental Results. a: -- ω_r^* , — $\hat{\omega}_r$ and …ω_r mech. rad/s. b: …ρ_r and — $\hat{\rho}_r$, elect. rad/s. c: $\Delta\rho_r$, elect. rad/s. d: $\hat{\psi}_r$, Web. e: …i_{sx} and — i_{sy}, A. f: …u_{sx} and — u_{sy}, V.